Structural isomerism-tuned magnetisation relaxation dynamics in lanthanide coordination complexes

Steen H. Hansen,*[†a] Christian D. Buch[†a] and Stergios Piligkos*[a]

The eigenspectrum and eigenvectors of the $^2F_{7/2}$ ground multiplets of two structural isomer coordination complexes, Yb(trenovan) (H_3trenovan = tris(((3-methoxysaliclidene)amino)ethyl)amine) and Yb(trenpvan) (H_3trenpvan = tris(((5-methoxysaliclidene)amino)ethyl)amine), were determined by use of magnetometry and electron paramagnetic resonance and luminescence spectroscopies. The two 4f complexes crystallise in the trigonal $P\bar{3}$ space group, have identical chemical formulas and differ only in the placement of the methoxy group on the aromatic ring of salicylaldehyde, with it being either ortho, Yb(trenovan), or para, Yb(trenpvan), to the phenoxo group. This structural isomerism is found to have a profound influence on the solid state static and dynamic magnetic properties of the complexes. In the bulk, both isomers display a combination of direct and raman magnetisation relaxation procceses, however, at vastly different rates. Magnetic dilution in an isostructural diamagnetic host supresses the occurrence of the direct procces suggesting that the direct process observed in the bulk originates from Yb(III) centres coupled by magnetic dipole interactions. The eigenspectrum, eigenvectors and spin lattice relaxation of Yb(trenpvan) are found to be closer to the ones found in Yb(trensal) (H_3trensal = tris(((saliclidene)amino)ethyl)amine) where the methoxy group is substituted by an H atom, than to those of Yb(trenovan) where the methoxy group is in the ortho position. Thus, the position of chemical modifications has a tremendous influence on the static and dynamic solid state magnetic properties of 4f coordination complexes. Our detailed study on single crystals, demonstrates that the rarely studied effect of modifications of the position of second coordination sphere chemical groups on the dynamic magnetic properties can in fact be used to chemically tune the magnetisation dynamics of 4f spin systems.

Introduction

The discovery in the early 1990's that a mixed valence dodecanuclear Mn coordination complex, Mn_{12}, was displaying magnetic bistability at the single molecule level,[1-3] laid the foundations for the research field of Single Molecule Magnets (SMMs).[4, 5] About a decade later, it was shown that mononuclear lanthanide (Ln) phthalocyanine complexes, $Ln(Pc)_2$ with Ln = Tb, Dy, displayed out-of-phase a.c.-magnetic susceptibility reflecting magnetic relaxation at the millisecond time scale.[6] Since this discovery, Ln coordination complexes have been demonstrated to display large coercive fields[7, 8] and spin-reversal energy barriers approaching 1000 K.[9, 10] Additionally, efforts have been dedicated to study the magnetic properties of 3d-4f complexes,[11, 12] toroidal moments in Ln systems,[13, 14] and of mononuclear[6, 8, 14-19] and polynuclear 4f complexes.[20, 21] In particular, Ln coordination complexes have been proposed for applications in Quantum Information Technologies (QITs).[16, 18, 22-29] Within the context of QITs, the number of performed quantum operations is limited by the phase memory time, T_m, and the operation (gate) time. The upper limit of T_m is defined by the spin-lattice relaxation time, T_1. Currently substantial efforts are devoted to developing molecular systems with long coherence times at temperatures higher than cryogenic ones. However, this effort is often hampered by the usually steep decrease of T_1 with temperature, T. This effect is often due to the exponential temperature dependence of the Orbach procces and to high exponents of the Raman processes. The exploitation of dynamic magnetic properties of molecular materials relies on the in-depth and detailed understanding of the fundamental factors that determine these.[23, 24, 30-37] It has long been recognised that the magneto-elastic coupling plays an important role for magnetisation relaxation. One phonon (Direct), two phonon (Orbach and Raman) and higher order phonon processes have been examined from first principles.[33] However, very few guidelines exist for chemical design of molecules with desired, tailored, dynamic magnetic properties as well as for understanding how small structural changes influence the dynamic magnetic properties[38, 39]. In the case of Ln complexes, Reinhart and Long proposed designing ligands which electrostatically complement the oblate or prolate nature of the lanthanide ground state electron density stabilising it, resulting to the increase of the Orbach barrier for magnetisation reversal.[40] Others have proposed that engineering of the Hamiltonian by use of high symmetry ligand fields can lead to quenching of QTM.[41, 42] Thus, to gain detailed insight into the dynamic magnetic properties and the fundamental factors that

[a] *Department of Chemistry, University of Copenhagen, DK-2100 Copenhagen, Denmark*

† These authors contributed equally to the experiments and writing of the article.
Electronic Supplementary Information (ESI) available

determine them, systematic and detailed investigations of the static and dynamic magnetic properties of numerus compounds are required.

In previous work we have investigated Yb(trensal) (H_3trensal = tris(((saliclidene)amino)ethyl)amine) as a potential molecular qubit.[16] Not only is Yb(trensal) a prototypical electronic qubit, but the hyperfine coupling between the electronic and nuclear spin can be used to implement error-correction protocols.[25] Additionally, single crystals of $Yb_{0.05}Lu_{0.95}$(trensal) were recently incorporated into circuit Quantum Electrodynamic Devices in view of the exploring the potential of such systems for the realisation of quantum processor prototypes.[26] However, the coherent magnetic properties of Yb(trensal) do not persist at temperatures higher than few tens of K. This is because T_m of Yb(trensal) is limited by the steep decrease of the spin lattice relaxation time, T_1, through its $T_1 \propto T^{-6}$ dependence. Given these very interesting properties displayed by Yb(trensal) we began to explore tuning of its static and dynamic magnetic properties by modifications of the trensal backbone. Herein, we thoroughly investigate the static and dynamic magnetic properties of two such Yb(trensal) derivatives Yb(trenovan) (H_3trenovan = tris(((3-methoxysaliclidene)amino) ethyl)amine) and Yb(trenpvan) (H_3trenpvan = tris(((5-methoxysaliclidene)amino)ethyl)amine). In these complexes the methoxy group is introduced either ortho or para to the phenoxide group. Through these substitutions, we study the electronic and structural effects on the magnetic properties associated to the addition of an electron donating group to a specific position of the aromatic ring. Both Ln(trenovan) and Ln(trenpvan) crystalize in a trigonal space group, analogous to the one Ln(trensal) crystalise in.[43-45] This makes comparison between Yb(trenovan), Yb(trenpvan) and Yb(trensal) relatively straightforward. The magnetic properties of the Ln(trenovan) series have previously been studied but never included detailed crystal field (CF) determination for the Yb(III) member of the family.[43] Herein, we present a multi-technique study of the CF and spin-lattice relaxation of bulk and dilute in the isostructural diamagnetic host Yb(trenovan) and Yb(trenpvan), including single-crystal continuous-wave electron paramagnetic resonance (c.w.-EPR) and luminescence spectroscopies and static and dynamic magnetisation measurements.

Experimental

Materials and methods

Tris-(2-aminoethyl)amine (tren), triflic acid, 2-hydroxy-3-methoxybenzaldehyde (o-vanilin), 2-hydroxy-5-methoxybenzaldehyde (p-vanilin), Yb_2O_3, Lu_2O_3 and all solvents used were obtained from commercial sources and used as received. $Yb(OTf)_3{\cdot}9H_2O$ and $Lu(OTf)_3{\cdot}9H_2O$ were prepared through a reaction between the corresponding oxide and aqueous triflic acid as described in the literature.[46]

CHN elemental analyses were performed using a FLASHEA 1112 at the Microanalytical Laboratory at the Department of Chemistry, University of Copenhagen. Matrix assisted laser desorption/ionization (MALDI) mass spectrometry was done using a Bruker Solarix XR 7T ESI/MALDI FT-ICR MS. For the mass spectra a dithranol matrix was used. Powder X-ray diffraction (PXRD) was measured using a BRUKER D8 ADVANCE powder diffractometer using a Cu Kα radiation source (λ = 1.5418 Å). X-band Electron paramagnetic resonance (EPR) was measured on a Bruker Elexsys E500 instrument equipped with an Oxford Instruments cryostat. Static and dynamic magnetic measurements were conducted on a Quantum Design MPMS-XL SQUID magnetometer. Prior to measurements crystalline samples were crushed to microcrystalline powders and fixed in *n*-hexadecane to avoid orientation of the sample in the magnetic field. χT measurements were corrected for the diamagnetism of the *n*-hexadecane using its literature magnetic susceptibility ($-187{\cdot}10^{-6}$ cm³/mol).[47] The diamagnetism of the sample was corrected for by using the approximation -0.5 x M_{sample} x 10^{-6} cm^3mol^{-1}.[48] Luminescence spectroscopy was performed on a Horiba-Jobin Yvon Fluorolog fluorimeter equipped with an InGaAs near-infrared (NIR) detector. An Oxford Instruments He flow cryostat was used for measurements at low temperatures.

Crystallography

Single-crystal X-ray diffraction was measured on a BRUKER D8VENTURE instrument at the Department of Chemistry, University of Copenhagen. The instrument is equipped with a Mo Kα high-brilliance IμS S3 radiation source (λ = 0.71073 Å) and a PHOTON 100 CMOS detector. Additionally, the instrument is equipped with an Oxford Instruments cryosystem allowing for structure determinations at both 120 and 300 K. The diffractometer was controlled using the APEX2 software package. Data reduction and absorption corrections were performed using SAINT[49] and SADABS,[50] respectively. The structures were solved using intrinsic phasing with SHELXT[51] and refined with SHELXL (least squares).[52, 53] For a graphical visualisation during the refinement process the OLEX2 program was used.[54, 55] All atoms except hydrogens have been refined with anisotropic ellipsoids. Hydrogen atoms were placed using the "Add H" command in OLEX2.

Synthesis of Yb(trenovan)

2-hydroxy-3-methoxybenzaldehyde (o-van, 0.19 g, 1.3 mmol) and $Yb(OTf)_3{\cdot}9H_2O$ (0.33 g, 0.42 mmol) were dissolved in MeCN (30 ml). Tren (0.061 g, 0.43 mmol) mixed with MeOH (2 ml) was added to the solution resulting in a change of colour to yellow. The solution was then heated to approximately 50 °C and Et_3N (0.25 ml) was added. The solution was stirred quickly and then left unstirred at room temperature until the next day. The crystalline precipitate was isolated and washed 3 times with ethanol and 2 times with diethyl ether.

Yield: 228 mg (75 %). Anal. Calcd for $C_{30}H_{33}N_4O_6Yb$: C, 50.14; H, 4.63; N, 7.80. Found: C, 50.62; H, 4.99; N, 7.31. MALDI mass spectrum: 720.19 *m/z* $[Yb(trenovan)H]^+$ and 742.17 *m/z* $[Yb(trenovan)Na]^+$ (Figure S1). IR $\tilde{\nu}_{C=N}$: $1623\ cm^{-1}$ (Figure S3). The phase purity of the polycrystalline product was verified by PXRD (Figure S5).

The magnetically dilute polycrystalline $Yb_{0.01}Lu_{0.99}$(trenovan) was prepared analogously to polycrystalline Yb(trenovan), using a molar ratio of 1:99 of $Yb(OTf)_3{\cdot}9H_2O$ and $Lu(OTf)_3{\cdot}9H_2O$, respectively. The phase purity of the microcrystalline product was verified by PXRD (Figure S7).

Preparation of $Yb_{0.03}Lu_{0.97}$(trenovan) single crystals

$Yb(OTf)_3{\cdot}9H_2O$ (2.8 mg; 3.6 µmol) and $Lu(OTf)_3{\cdot}9H_2O$ (93 mg; 119 µmol) were dissolved in MeCN (20 ml). To this o-van (55 mg; 361 µmol) in MeOH (20 ml) was added. To the pale yellow solution tren (18 mg; 123 µmol) in MeOH (1 ml) was added and the resulting yellow solution was stirred for a short while. Then, Et_3N (0.1 ml) was added and the solution was stirred shortly and then left at room temperature without stirring. Within a week millimetre sized crystals formed.

Synthesis of Yb(trenpvan)

2-hydroxy-5-methoxybenzaldehyde (p-van, 0.20 g; 1,3 mmol) was dissolved in MeOH (20 ml). $Yb(OTf)_3{\cdot}9H_2O$ (0.34 mg; 0.43 mmol) and tren (62 mg, 0.42 mmol) were then added under stirring. The resulting mixture was stirred for 15 min. Et_3N (0.2 ml) was added resulting in a yellow precipitate forming. The yellow precipitate was filtered, dried and recrystallized by dissolution in 40 ml hot MeCN and subsequently removing the solvent by boiling until a precipitate formed, at which point the heating was stopped. This resulted in yellow elongated hexagonal crystals suitable for single crystal diffraction.
Yield: 110 mg (35 %). Anal. Calcd for $C_{30}H_{33}N_4O_6Yb$: C, 50.07; H, 4.76; N, 7.79. Found: C, 50.13; H, 4.71; N, 7.56. MALDI mass spectrum: 720 *m/z* $[Yb(trenpvan)H]^+$ (Figure S2). IR $\tilde{\nu}_{C=N}$: $1632\ cm^{-1}$ (Figure S4). The phase purity of the microcrystalline product was checked by PXRD (Figure S6).
Magnetically dilute $Yb_{0.01}Lu_{0.99}$(trenpvan) was prepared analogously to Yb(trenpvan), however, using a molar ratio of 1:99 of $Yb(OTf)_3{\cdot}9H_2O$ and $Lu(OTf)_3{\cdot}9H_2O$, respectively. The phase purity of the microcrystalline product was verified by PXRD (Figure S8).

Preparation of $Yb_{0.05}Y_{0.95}$(trenpvan) single crystals

Single crystals of $Yb_{0.05}Y_{0.95}$(trenpvan) were prepared analogously to Yb(trenpvan), however, a molar ratio of 5:95 of $Yb(OTf)_3{\cdot}9H_2O$ and $Y(OTf)_3{\cdot}9H_2O$ was used. The polycrystalline precipitate was redissolved in MeCN. Large single crystals suitable for single-crystal EPR formed by slow evaporation of the resulting solution.

Results and discussion

Crystal structure

Yb(trenovan) and Yb(trenpvan) both crystallise in the trigonal space group $P\bar{3}$ as hexagonal prisms. In the unit cell, the crystallographic and molecular threefold axes are coincident resulting in one third of the molecule being contained in the asymmetric unit (Figure S9). This is similar to the parent complex Yb(trensal) which crystallises in the trigonal space group $P\bar{3}c1$.[56-58] However, in the case of Yb(trensal) four molecules are contained in the unit cell whereas the crystal structures of Yb(trenovan) and Yb(trenpvan) only contain two molecules of opposite chirality (the ligand scaffold either forms a Δ or Λ screw axis around the Yb(III) centre). Although the structure of Yb(trensal) is not in the same space group as the one of Yb(trenovan) and Yb(trenpvan), the intermetallic Yb-Yb distances are very similar in the three structures. At 120 K the two shortest Yb-Yb distances in Yb(trensal) are 7.607 and 8.154 Å, while in Yb(trenovan) they are 8.185 and 8.265 Å, and in Yb(trenpvan) they are 7.545 and 8.590 Å.

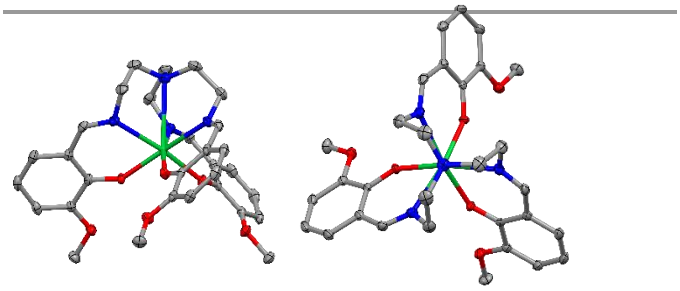

Figure 1 Left: Crystal structure obtained at 120 K of Yb(trenovan) seen from the side (left) and from the top along the threefold axis (right). Hydrogens have been omitted for clarity and thermal ellipsoids have been set to 50 %. Colour scheme: C, gray; O, red; N, blue and Yb, green. Similar orientations of the Yb(trenpvan) structure can be found in Figure S10.

The unit cell dimensions for the two crystal structures are very similar with the unit cell volume being 1387.6 $Å^3$ and 1420.0 $Å^3$ for Yb(trenovan) and Yb(trenpvan), respectively (Table S1). The geometry of the complexes is reflected in the unit cell dimensions. The long and narrow Yb(trenovan) has smaller *a* and *b*, but larger *c*, unit cell lengths than the flattened Yb(trenpvan) (Figures 1 and S10, and Table S1).
The addition and position of the methoxy group affects the ligand to Yb(III) bond lengths in different ways. The Yb-N_{imine} and Yb-O bond lengths are little affected by the methoxy group varying by only 0.017(4) and 0.005(2) Å between the three different complexes, respectively (Table 1). On the contrary, the Yb-N_{apical} bond is greatly affected by the position of the methoxy group varying by 0.218(6) Å (8 %) going from Yb(trenpvan) to Yb(trenovan) (Table 1). Interestingly, in the solid state, the position of the methoxy group affects the Yb ligand bond lengths to a greater extent than just substituting one of the hydrogens in Yb(trensal) for the methoxy group. For instance, the Yb-N_{apical} bond is shortened by 0.048 Å going from Yb(trensal) to Yb(trenpvan), while it is elongated by 0.172 Å going from Yb(trensal) to Yb(trenovan) (Table 1). Thus, a subtle chemical modification can lead to significant structural variations, in the solid state. In addition to bond lengths, bond and torsions angles in the complexes are also greatly affected by the methoxy group isomerism. Again, these angles are more affected by methoxy position isomerism rather than by the substitution of an H for the methoxy group (Table 1). For instance, the angles found in Yb(trenpvan) are much closer to the ones in Yb(trensal) than the ones in Yb(trenovan) (Table 1). This is also evident when the structures are overlaid (Figures 2 and S11 – S12).

Table 1 Selected bond lengths and angles in Yb(trensal), Yb(trenovan) and Yb(trenpvan) at 120 K.

Compound	Yb(trensal)[58]	Yb(Trenovan)	Yb(trenpvan)
Yb-N_{apical} (Å)	2.705	2.875(3)	2.657(3)
Yb-N_{imine} (Å)	2.431	2.420(2)	2.414(2)
Yb-O (Å)	2.166	2.171(1)	2.166(1)
∠(N_{apical}-Yb-N_{imine})	66.58	63.93(4)	68.04(4)
∠(N_{apical}-Yb-O)	122.06	120.36(4)	122.45(4)
Torsion angle	138.40	142.34(12)	134.23(13)

The structure of Yb(trenovan) has previously been determined at room temperature.[44] This structure is very similar to the one presented in this work, with only slight changes to the bond lengths. For instance, Yb-N_{apical} changes from 2.875(3) to 2.902 Å and Yb-O changes from 2.171(1) to 2.166 Å when going from the structure at 120 K to the one at room temperature.

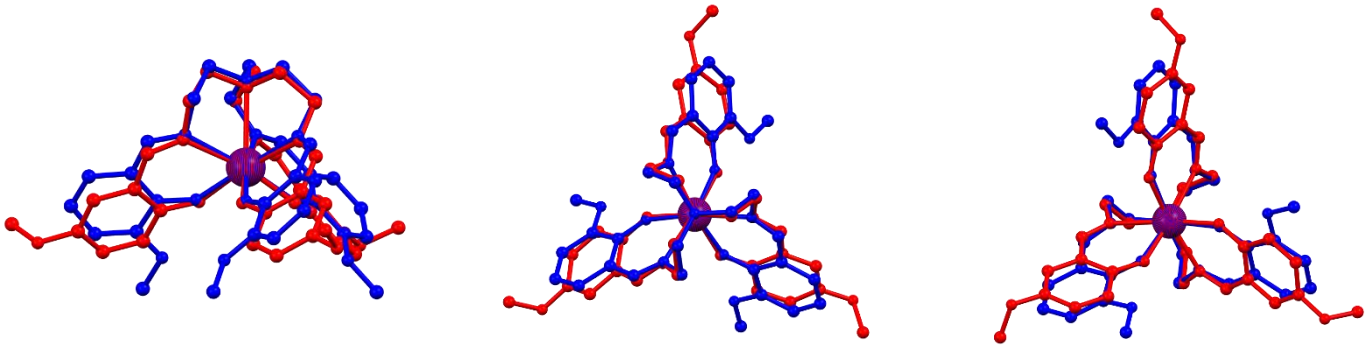

Figure 2 Structural overlay of the crystal structures of Yb(trenovan) in blue and Yb(trenpvan) in red viewed from the side (left), top (middle) and bottom (right).

Static electronic properties

The static electronic properties of Yb(trenovan) and Yb(trenpvan) were studied via a multi technique approach involving magnetic susceptibility and variable-temperature–variable-field (VTVB) magnetisation, luminescence, and single crystal continuous wave electron paramagnetic resonance (c.w.-EPR) measurements. These techniques in conjunction allow for the detailed determination of the eigenvalues and eigenvector composition of the ground $^2F_{7/2}$ term of the two systems.

D.C. magnetic susceptibility, χ, measurements were performed in a static magnetic field, B, of 1000 Oe and in the temperature, T, range 2 – 270 K, with $\chi = M / B$. The χT curves of Yb(trenovan) and Yb(trenpvan) show very similar behaviour (Figure S13). Neither Yb(trenpvan) nor Yb(trenovan) reach the Curie constant of Yb (2.57 $cm^3mol^{-1}K$), suggesting a splitting of the Kramers sublevels of the ground $^2F_{7/2}$ term of the order of magnitude or higher than the thermal energy available at 270 K. Similar observations have been made for many other Yb containing Ln(trensal) derivatives.[43, 58-60] The χT products of Yb(trenovan) and Yb(trenpvan) (1.87 and 1.83 $cm^3mol^{-1}K$, respectively) are close to the one of Yb(trensal) (2.0 $cm^3mol^{-1}K$) or of other Yb(trensal) derivatives such as Yb(trenomyl) (1.84 $cm^3mol^{-1}K$).[59] This is to be expected due to the close structural resemblance between these derivatives.

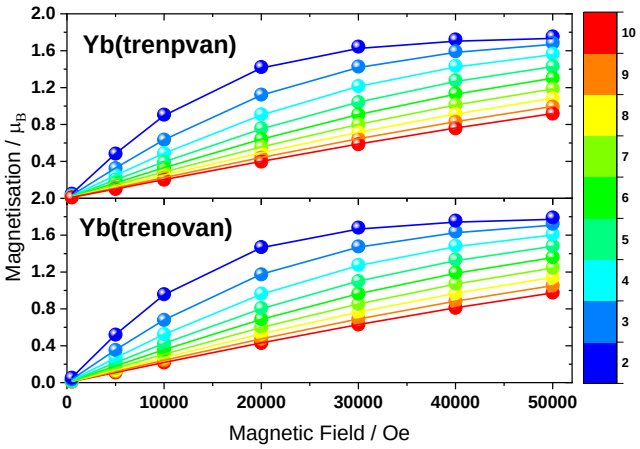

Figure 3 VTVB magnetisation measurements of Yb(trenovan) and Yb(trenpvan). Experiment in scatter and the best fit (solid lines) obtained as described in the text.

Reduced magnetisation plots of the complexes show no nesting (Figures S14 – S15), suggesting a well isolated ground doublet in agreement with the large spitting of the m_j sublevels of the ground $^2F_{7/2}$ term at zero applied magnetic field, suggested by the χT measurements.

The VTVB measurements of Yb(trenovan) and Yb(trenpvan) are very similar. At 2 K and 5 T the magnetisation of both complexes reaches its largest value: 1.79 and 1.75 μ_B for Yb(trenovan) and Yb(trenpvan), respectively. The larger magnetisation value of Yb(trenovan) suggests a larger g-factor, which is also confirmed by EPR spectroscopy (*vide infra)*.

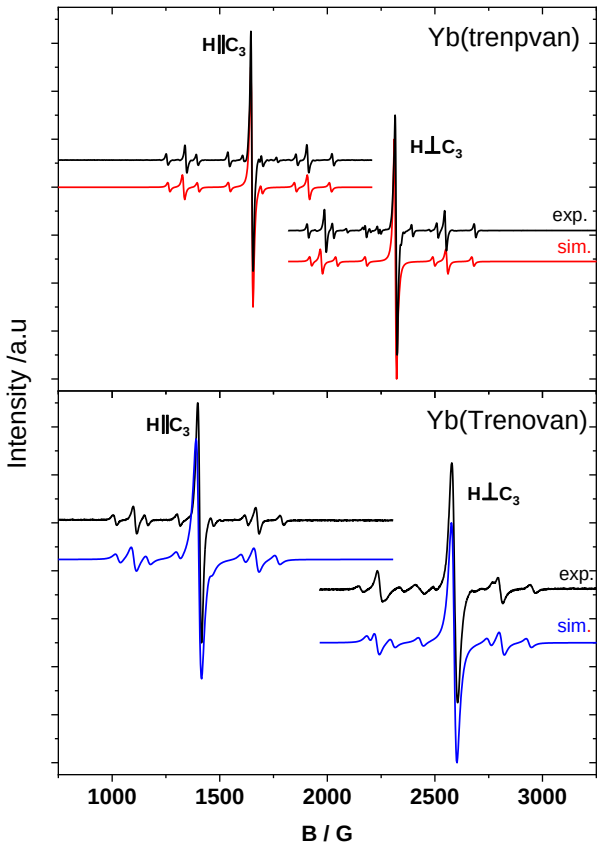

Figure 4 X-band c.w.-EPR((9.6 GHz) spectra of $Yb_{0.05}Lu_{0.95}$(trenpvan) (top) and $Yb_{0.03}Lu_{0.97}$(trenovan) (bottom). Experiments are in black while the best fits as described in the main text are in red and blue for Yb(trenpvan) and Yb(trenovan), respectively. The spectra were recorded at 9 K and 4 K for Yb(trenovan) and Yb(trenpvan), respectively.

C.w.-EPR spectra were measured on single crystals of $Yb_{0.03}Lu_{0.97}$(trenovan) and $Yb_{0.05}Lu_{0.95}$(trenpvan). Using a goniometer the crystals were oriented with the molecular C_3 axis either parallel or perpendicular to the magnetic field, B_0. The spectra were measured at 4 K for Yb(trenpvan) and 9 K for Yb(trenovan). EPR spectroscopy is very sensitive to the composition of the ground doublet of the Yb(III) ion allowing the precise determination of the eigenvector composition of Yb(trenovan) and Yb(trenpvan). In addition to variations in the electronic state eigenvectors, X-band EPR spectroscopy (~ 0.3 cm^{-1}) also allows the study of the change in hyperfine coupling between the electron and nuclear spin upon going from Yb(trenovan) to Yb(trenpvan) *via* Yb(trensal). Yb has seven natural isotopes of which five possess no nuclear spin (I = 0), while the isotopes ^{171}Yb and ^{173}Yb have I = 1/2 and I = 5/2, respectively. Given that the reduced magnetisation (Figures S14 – S15) and luminescence (*vide infra)* measurements suggest a thermally isolated ground Kramers doublet for both Yb(trenovan) and Yb(trenpvan), the EPR spectra of these were modelled as originating from effective spin-1/2 systems.

Table 2 EPR parameters of Yb(trensal),[61] Yb(trenovan) and Yb(trenpvan)

Compound	$g_\parallel$	$g_\perp$	$A_\parallel$ [MHz]	$A_\perp$[MHz]
Yb(trensal)	4.29	2.90	936*	672*
Yb(trenpvan)	4.16	2.96	865	622
Yb(trenovan)	4.89	2.65	1012	548

*These values are only for the I = 1/2 isotope

To this purpose we used the following Hamiltonian:

$$\hat{H} = \mu_B \cdot B_0 \cdot \tilde{g} \cdot \hat{S} + \hat{S}\mathrm{A}\hat{I}$$

with μ_B being the Bohr magneton, $\tilde{g}$ being the diagonal g-tensor, $\hat{S}$ being the spin operator, A being the diagonal hyperfine coupling tensor and $\hat{I}$ being the nuclear spin operator. Since both Yb(trenovan) and Yb(trenpvan) are axial systems, we set $g_z = g_\parallel$ and g_x=g_y=$g_\perp$. Likewise, the hyperfine coupling to the nucleus is described by a diagonal A tensor with $A_z = A_\parallel$ and $A_x = A_y = A_\perp$. EasySpin[62] was used to model the data to the Hamiltonian above. The determined g- and A-values are given in Table 2. The reported hyperfine is the coupling to most abounded ^{173}Yb nuclei, the coupling to ^{171}Yb is obtained by scaling the value with the ratio of gyromagnetic moment of the two isotopes.

The obtained g-values clearly differ, being relatively similar between Yb(trenpvan) and Yb(trensal), while Yb(trenovan) is significantly more anisotropic in terms of g-values. This is reminiscent of the crystal structures, where Yb(trensal) and Yb(trenpvan) were structurally more similar between them than to Yb(trenovan).

A purely axial system with a ground doublet of m_j = ±7/2 would result in an effective $g_\parallel$ value of 8 and an effective $g_\perp$ value of zero. Hence, the ground Kramers doublets contain significant amounts of mixing with other m_j states. Similar results on $g_\parallel$ and $g_\perp$ of Yb(trenovan) were previously obtained on bulk polycrystalline samples at 220 GHz. However, no clear hyperfine couplings were observed in those samples.[43]

The dipole-dipole and Fermi contact terms of the hyperfine interaction scale both as: $A \propto g$. Hence, the hyperfine interaction scales with the electronic g-factors.[63] By correcting for this by taking the ratio A/g, fairly similar values of 218, 208 207 Mhz ($C_3 \parallel B_0$) and 232, 210 and 207 MHz ($C_3 \perp B_0$) for Yb(trensal), Yb(trenovan) and Yb(trenpvan), respectively, were obtained. This suggests that the electron interaction with the nucleus is nearly unperturbed by the substituent on the benzene ring and the perturbations it induces on bond lengths and angles. It has to be noted that the small additional peaks in the c.-w. EPR spectra that are not accounted for by the simulations, are attributed to sites where Yb(III) ions are first neighbours and coupled by dipolar interactions, as it has been established for Yb(trensal) by c.-w. and pulse EPR.[23]

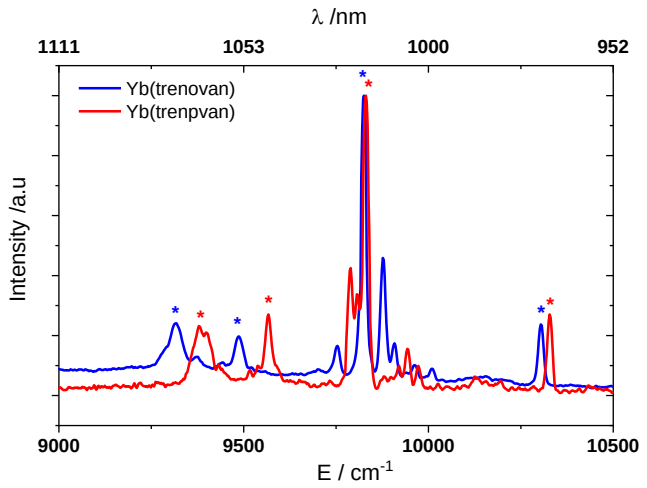

Figure 5 Luminescence spectra of polycrystalline Yb(trenovan) and Yb(trenpvan) powders measured at 30 K. For both spectra an excitation wavelength of 400 nm was used. Electronic transitions are marked with *.

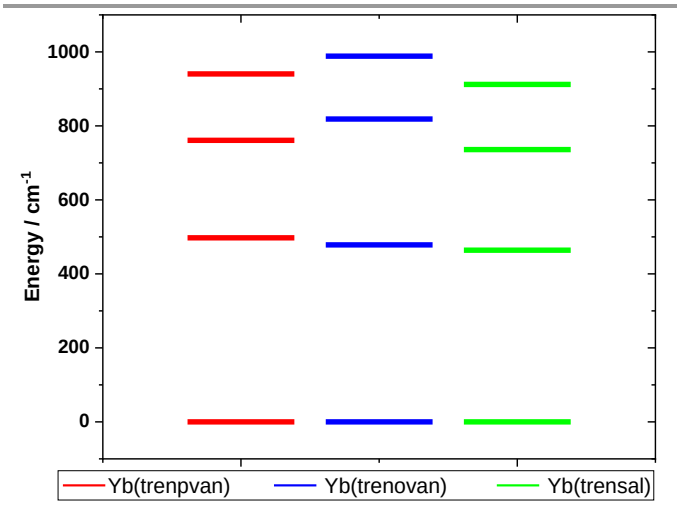

Figure 6 Energy level diagram of the ground multiplet $^2F_{7/2}$ of Yb(III) in Yb(trenpvan), Yb(trenovan) and Yb(trensal). The energy levels of Yb(trenovan and Yb(trenpvan) are calculated based on the best-fit parameters given in the main text. While those of Yb(trensal) are obtained from literature.[58]

Emission spectra of Yb(III) provide information on the relative energy splittings of the Kramers doublets of the $^2F_{7/2}$ ground term. Luminescence spectra of Yb(trenovan) and Yb(trenpvan) were measured at 30 K, to ensure sharp bands, hence allowing very precise determination of the above-mentioned energy splittings. The spectra were obtained by excitation at the highly absorbing ligand $\pi \rightarrow \pi^*$ absorption band at 400 nm. This excitation wavelength was chosen to avoid higher order diffraction from the diffraction grating of the excitation monochromators overlapping with the investigated spectral range. The resulting emission spectra are very similar to the ones of Yb(trensal), both in energy separations and intensities. Hence, the electronic transitions (marked with * in the spectra of Figure 5) are readily assigned based on our previous work on Yb(trensal).[58] The additional smaller emission bands observed originate from the vibronic structure of the $^2F_{7/2}$ ground term. Similar bands have also been observed for Yb(trensal). The resulting energy level diagrams extracted for both Yb(trenpvan) and Yb(trenovan) are shown in Figure 6 along with the one for Yb(trensal). The similarity in the crystal field splitting of the three compounds is clearly visible from Figure 6, with Yb(trenpvan) and Yb(trensal) being nearly identical while Yb(trenovan) shows a slightly larger total energy splitting of 989 cm^{-1}, compared to 941 cm^{-1} for Yb(trenpvan) and 913 cm^{-1} for Yb(trensal).

The multi-technique approach used herein allows the determination of the crystal field (CF) parameters of the $^2F_{7/2}$ ground term for both Yb(trenovan) and Yb(trenpvan). To this purpose, we simultaneously fitted the single crystal c.w.-EPR spectra (with $C_3 \parallel B_0$ and $C_3 \perp B_0$), the VTVB magnetisation measurements, the temperature dependence of the χT product and the luminescence spectra to the following Hamiltonian:

$$\hat{H} = \mu_B \boldsymbol{B} g_J \hat{\boldsymbol{J}} + \sum_{k,-k\leq q\leq k} B_k^q \, \hat{\boldsymbol{O}}_k^q$$

where the first term expresses the Zeeman interaction and the second term the CF splitting in Stevens parametrisation, B_k^q being the CF parameter and $\hat{\boldsymbol{O}}$ the associated CF operator (with k = 2, 4 or 6 for J = 7/2 and $-k \leq q \leq k$), in the basis defined by the four Kramers doublets of the ground $^2F_{7/2}$ multiplet of Yb(III). This leads, in general, to 27 operators in total and hence 27 Stevens CF parameters. However, in the case of Yb(trenovan) and Yb(trenpvan) the threefold symmetry limits the number of parameters to only 9, namely $B_2^0, B_4^0, B_4^{\pm 3}, B_6^0, B_6^{\pm 3}, B_6^{\pm 6}$. Since the reference frame of the system can be chosen arbitrarily, B_4^{-3}, for example, can be set to zero by choosing an appropriate coordinate system, limiting the amount of parameters to 8. Using this approach excellent fits to all experimental data are obtained (Figures 3, 4 and S13). The derived model fits the emission data within 2 cm^{-1} and the EPR spectra within 5 G. The obtained Stevens parameters can be found in Table S7. The resulting eigenvector compositions of the ground Kramers doublet show generally similar structure with the most significant differences being the contribution of the ±1/2 and ±5/2 while the ±7/2 stays almost constant (Tables S8 – S9). This is due to the relative size of the $B_6^{\pm 6}$ parameter relative to the $B_6^{\pm 3}$ and B_4^{+3} parameters.

Usually, a larger value of effective $g_{//}$ is correlated to the purity of the eigenvectors in terms of m_j composition and thus to the axiality of the system, where the maximum effective $g_{//}$ corresponds to the ground doublet being composed exclusively by the maximum (absolute value) m_j projections. However, for the systems studied herein, the difference in the observed

effective g-values is mainly a consequence of the relative contributions from the m_j = ± 1/2 and m_j = ± 5/2 components, the contribution from the m_j = ± 7/2 components being essentially constant across the three complexes as shown in table 3.

Table 3. Eigenvector composition of the ground doublet in Yb(trenovan), Yb(trenpvan) and Yb(trensal).

	Yb(trenovan)		Yb(trenpvan)		Yb(trensal)	
$\|7/2\rangle$	62	-	60	-	58	-
$\|5/2\rangle$	-	7	-	16	-	12
$\|3/2\rangle$	-	-	-	-	-	-
$\|1/2\rangle$	31	-	25	-	30	-
$\|-1/2\rangle$	-	31	-	25	-	30
$\|-3/2\rangle$	-	-	-	-	-	-
$\|-5/2\rangle$	7	-	16	-	12	-
$\|-7/2\rangle$	-	62	-	60	-	58

The eigenvector compositions for Yb(trenovan) and Yb(trenpvan) were obtained by simultaneously fitting the luminescence spectra, single crystal EPR spectra, the temperature dependence of the χT product and the VTVB measurements, as described in the main text. The composition for Yb(trensal) was obtained from literature.[61]

Dynamic magnetic properties

The spin lattice relaxation of the two derivatives was investigated by measuring the dynamic magnetic susceptibility (χ' and χ'') as a function of the frequency of an oscillating magnetic field, with an applied static magnetic field ranging from 0 – 4000 Oe (Figures S16 and S19). When no magnetic field is applied none of the complexes shows a χ'' signal, similar to what observed for Yb(trensal).[58] Upon applying an external magnetic field, a χ'' signal emerges for both derivatives. Although Yb(trenovan) and Yb(trenpvan) are structural isomers and only differ by the position of the methoxy group, the field dependence of their a.c. susceptibility is very different. Yb(trenpvan) shows minimal frequency variation of the position of χ'' in the explored field range. On the contrary, for Yb(trenovan) χ'' is strongly influenced by changes in the magnetic field, with χ'' diminishing at high frequencies with increasing static magnetic field and increasing at low frequencies (Figures S16 and S19). The relaxation time, τ, was obtained by measuring the a.c. susceptibility of Yb(trenovan) and Yb(trenpvan) in an applied static magnetic field of 500 Oe in the temperature range 1.9 – 4.7 and 1.9 – 6.8 K, respectively (Figures S17 and S20). The magnetic field was set to 500 Oe as this is the optimum field for measuring χ'' for Yb(trenovan) and χ'' of Yb(trenpvan) shows little dependence on the applied magnetic field. Using a generalized Debye model, τ was extracted for both complexes (Figure 7 and Tables S2 and S4) by use of CC-FIT2.[64, 65] In our previous study of Yb(trensal), a combination of direct and Raman processes were found to describe the spin-relaxation dynamics. Hence, a similar model was used herein:

$$\tau^{-1} = D \cdot T + C \cdot T^n$$

where the first term describes a non-phonon bottlenecked direct process while the second term describes the two phonon Raman process. The experimental data were fitted to the above-mentioned relaxation model, resulting in the best-fit parameters given in Table 4. At low temperatures the direct process is the dominant process, whereas, at higher temperatures the Raman process becomes the dominant one.

Table 4. Best fit parameters for the temperature dependence of the spin lattice relaxation (τ) of Yb(trenovan), Yb(trenpvan) and Yb(trensal) fitted to a model containing a direct and a Raman process as described in the main text.

Compound	D (s^{-1} K^{-1})	C (s^{-1} K^{-n})	n
Yb(trensal)	258	0.15	6.2
Yb(trenpvan)	92.5(3)	0.0037(6)	8.1(1)
$Lu_{0.99}Yb_{0.01}$(trenpvan)	-	0.0041(1)	7.6(1)
Yb(trenovan)	355(3)	2.3(2)	6.2(1)
$Lu_{0.99}Yb_{0.01}$ (trenovan)	-	6.9(1)	4.7(1)

The parameters for Yb(trensal) are obtained from literature.[58]

This is similar to what has been observed in Yb(trensal), the relaxation fit of which is included as a green line in Figure 7. The fitted direct process coefficient, D, of Yb(trenovan) (335 s^{-1} K^{-1}) is fairly similar to the one obtained for Yb(trensal) (258 s^{-1} K^{-1}) while Yb(trenpvan) (28.5 s^{-1} K^{-1}) displays an order of magnitude slower direct process. In terms of the Raman process Yb(trenovan) and Yb(trensal) are again very similar having the same Raman exponent, while Yb(trenpvan) shows a much more different Raman exponent. To gain further insight into the spin dynamics of the systems and to reduce the effect of neighbours the temperature dependence of τ was measured at 500 Oe on magnetically dilute $Lu_{0.99}Yb_{0.01}$(trenpvan) and $Lu_{0.99}Yb_{0.01}$ (trenOvan). As expected by minimising the dipolar couplings to neighbours and thereby the magnetic noise in the neighbouring environment of each spin, τ is increased at all temperatures. The largest change in τ upon dilution is seen at low temperatures, where τ is changed by almost one order of magnitude for Yb(trenovan) and almost two orders of magnitude for Yb(trenpvan). This regime is governed by the direct process in the concentrated samples. However, upon dilution the direct process regime changes dramatically. In the case of Yb(trenovan) no sign of the direct process regime is visible down to 1.9 K in $Lu_{0.99}Yb_{0.01}$(trenovan), while in $Lu_{0.99}Yb_{0.01}$(trenpvan) the direct process is only dominating up to 2.4 K compared to 4 K in the concentrated sample. This indicates that what in concentrated samples is perceived as a direct process, it is in fact a relaxation mechanism occurring between dipolarly coupled neighbours. Hence, it is not an intrinsic property of the individual molecules. These observations are in agreement with our recent study of $Yb_{0.01}Lu_{0.99}$(trensal) where the spin lattice relaxation was determined independently for single-ion and dipolar-interaction-coupled Yb(III) sites in a single crystal of $Yb_{0.01}Lu_{0.99}$(trensal) by X-band pulsed EPR.[23] In this recent study, we showed that magnetic dipole coupled Yb(III) sites show relaxation times with a $\tau \propto T^{-0.8}$ dependence at low temperatures and a $\tau \propto T^{-5.1}$ dependence at higher temperatures. On the contrary the single-ion lines show a constant temperature dependence of $\tau \propto T^{-5.4}$ across the investigated temperature range (2 – 18 K), indicating that the direct process is linked to magnetic dipole coupled Yb(III) sites. For both complexes the Raman process is still operative after dilution and less affected by the dilution than the direct process indicating that the observed Raman process in the bulk sample is an intrinsic property of individual molecules in the lattice. The

Raman parameters for Yb(trenpvan) are very similar to the ones observed for $Lu_{0.99}Yb_{0.01}$(trenpvan). Contrary, the Raman parameters for Yb(trenovan) differ more between the diluted and bulk samples, likely due to the direct process dominating spin relaxation in the whole studied temperature interval, of the bulk sample rendering determination of the Raman parameters difficult.

The determined Raman parameters differ significantly between the three compounds. The direct process prefactor, D, varies about 2 orders of magnitude between Yb(Trenovan) and Yb(Trenpvan) with Yb(trensal) being somewhat intermediate between the two. Likewise, the Raman pre-exponent is also much smaller for Yb(trenpvan). However, the Raman exponent, *n*, is larger for Yb(trenpvan), resulting in a faster drop in relaxation times with rising temperatures.

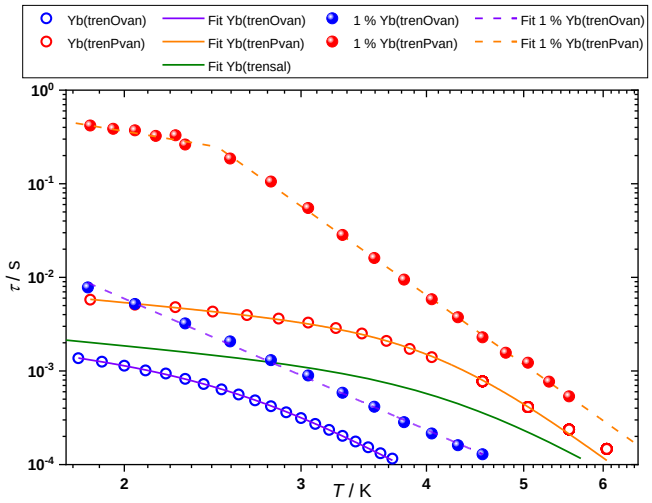

Figure 7. Temperature dependence of the spin lattice relaxation time (τ) of Yb(trenovan) and Yb(trenpvan) (scatter), and $Yb_{0.01}Lu_{0.01}$(trenovan) and $Yb_{0.01}Lu_{0.01}$(trenpvan) (hollow symbols) with an applied magnetic field of 500 Oe. The best fits to the relaxation times based on the models described in the main text are shown as full or dashed lines. For Yb(trensal) a simulation of the temperature dependence based on literature[61] values for its direct and Raman process is shown as a green line.

The stark difference in relaxation dynamics is surprising given the very similar structures of the three compounds and similar eigenvector composition (Tables 3 and S7-9). The Raman parameters *C* and *n* would be expected to be similar for the investigated compounds. These parameters describe the shape of the phonon density of states and the spin-phonon coupling to these.[66] The acoustic phonons are expected to be nearly identical since the intermolecular interactions are very similar, the space group is the same and the molecules are of exactly the same mass. The optical phonons seen using IR spectroscopy (Figures S3 and S4) are very different in the low-energy part of the IR spectrum. This suggests that the optical phonons might be surprisingly different giving rise to different temperature dependencies and preexponential factors.

The large difference of magnetisation relaxation dynamics between these very closely related compounds highlights the need for a much better understanding of how structural and electronic factors influence Raman relaxation. This will be further examined in future work by investigation of the vibrations and their coupling to the magnetic moment by Far Infra-Red Magneto-Spectroscopy (FIRMS), in line with our similar previous studies on Yb(trensal).[31]

Conclusions

The structural and static and dynamic electronic properties of the structural isomers Yb(trenovan) and Yb(trenpvan) were investigated by a multitechnique approach. These complexes show great structural similarities to the parent Yb(trensal), both retaining the same first coordination sphere and symmetry around the Yb(III) ion. Interestingly, the introduction of the methoxy group perturbs the coordination environment around Yb(III) less than changing the position of the methoxy group from ortho to para. For instance, the Yb-N_{apical} distance is elongated by 0.22 Å going from Yb(trenpvan) to Yb(trenovan) and by 0.17 Å going from Yb(trensal) to Yb(trenovan). Similarly the EPR g values of Yb(trenovan) and Yb(trenpvan) differ more than either of the derivatives compared to Yb(trensal). This indicates that the position of the methoxy group, rather than its introduction onto the ring system, affects the Yb centre's properties the most, as clearly reflected in both the determined effective g-factors and Raman exponents. Thus, fine-tuning of the eigenstates of Ln coordination complexes can be achieved not only by addition of various chemical groups on the parent complexes but also by variation of the position of chemical functions belonging to the second coordination sphere, thereby offering an additional handle to tune the spin dynamics of Ln based systems. The ability to control the Raman process is particularly important for 4f based molecular qubits. In these systems the phase memory time, T_m, gets limited by the spin-lattice relaxation time, T_1, at high temperatures. This is for instance seen in $Yb_{0.01}Lu_{0.99}$(trensal) which functions as a qubit up to 20 K at which temperature it gets T_1 limited. By lowering the Raman exponent and minimizing the preexponential factor of the relaxation rate, derivatised Yb(trensal) analogues could possibly be engineered to act as qubits at higher operating temperatures. Furthermore, we show herein that tuning of the eigenvector composition, thus, of the effective g-factors, results in different magnitudes (tuning) of the hyperfine coupling to the Yb nuclear spin. Control over the hyperfine interaction is particularly important in systems where the nuclear spin states are used for the implementation of quantum error-correction protocols, as has previously been demonstrated in the case of Yb(trensal).[25] Possessing the ability to fine-tune the hyperfine coupling will allow for greater control of the time scale involved in the addressing of nuclear spin states.

Author Contributions

The project was conceived by all three authors who also jointly wrote the manuscript. SHH collected the EPR and luminescence data, CDB collected the magnetisation data, measured and processed single crystal x-ray data. SHH analysed all data.

Conflicts of interest

There are no conflicts to declare.

Acknowledgements

We thank the Novo Nordisk Foundation for research grant NNF20OC0065610 under the Natural and Technical Sciences programme.

Notes and references

Crystallographic data (including structure factors) for Yb(trenovan) and Yb(trenpvan) have been deposited with the Cambridge Crystallographic Data Centre: CCDC 2234248 and 2236956 for Yb(trenovan) at 100 K and 300 K, respectively, and 2234249 and 2236957 for Yb(trenpvan) at 100 K and 300 K, respectively. Copies of the data can be obtained, free of charge, on application to Cambridge Crystallographic Data Centre, 12 Union Road, Cambridge CB2 1EZ, UK, (fax: +44-(0)1223-336033 or email: deposit@ccdc.cam.ac.uk).

1. T. Lis, Preparation, structure, and magnetic properties of a dodecanuclear mixed-valence manganese carboxylate, *Acta Crystallographica Section B*, 1980, **36**, 2042-2046.
2. R. Sessoli, H. L. Tsai, A. R. Schake, S. Wang, J. B. Vincent, K. Folting, D. Gatteschi, G. Christou and D. N. Hendrickson, High-spin molecules: [Mn12O12(O2CR)16(H2O)4], *Journal of the American Chemical Society*, 1993, **115**, 1804-1816.
3. R. Sessoli, D. Gatteschi, A. Caneschi and M. A. Novak, Magnetic bistability in a metal-ion cluster, *Nature*, 1993, **365**, 141-143.
4. D. Gatteschi, R. Sessoli and J. Villain, *Molecular nanomagnets*, Oxford University Press, New York, 2006.
5. R. Winpenny, *Single-Molecule Magnets and Related Phenomena*, Springer-Verlag Berlin Heidelberg, Berlin, Heidelberg, 2006.
6. N. Ishikawa, M. Sugita, T. Ishikawa, S.-y. Koshihara and Y. Kaizu, Lanthanide Double-Decker Complexes Functioning as Magnets at the Single-Molecular Level, *Journal of the American Chemical Society*, 2003, **125**, 8694-8695.
7. S. Demir, M. I. Gonzalez, L. E. Darago, W. J. Evans and J. R. Long, Giant coercivity and high magnetic blocking temperatures for N23− radical-bridged dilanthanide complexes upon ligand dissociation, *Nature Communications*, 2017, **8**, 2144.
8. C. A. P. Goodwin, F. Ortu, D. Reta, N. F. Chilton and D. P. Mills, Molecular magnetic hysteresis at 60 kelvin in dysprosocenium, *Nature*, 2017, **548**, 439-442.
9. S. T. Liddle and J. van Slageren, Improving f-element single molecule magnets, *Chem Soc Rev*, 2015, **44**, 6655-6669.
10. D. N. Woodruff, R. E. Winpenny and R. A. Layfield, Lanthanide single-molecule magnets, *Chem Rev*, 2013, **113**, 5110-5148.
11. G. Karotsis, M. Evangelisti, S. J. Dalgarno and E. K. Brechin, A Calix[4]arene 3d/4f Magnetic Cooler, *Angewandte Chemie International Edition*, 2009, **48**, 9928-9931.
12. G. Karotsis, S. Kennedy, S. J. Teat, C. M. Beavers, D. A. Fowler, J. J. Morales, M. Evangelisti, S. J. Dalgarno and E. K. Brechin, [MnIII4LnIII4] Calix[4]arene Clusters as Enhanced Magnetic Coolers and Molecular Magnets, *Journal of the American Chemical Society*, 2010, **132**, 12983-12990.
13. J. Tang, I. Hewitt, N. T. Madhu, G. Chastanet, W. Wernsdorfer, C. E. Anson, C. Benelli, R. Sessoli and A. K. Powell, Dysprosium Triangles Showing Single-Molecule Magnet Behavior of Thermally Excited Spin States, *Angewandte Chemie International Edition*, 2006, **45**, 1729-1733.
14. J. Luzon, K. Bernot, I. J. Hewitt, C. E. Anson, A. K. Powell and R. Sessoli, Spin Chirality in a Molecular Dysprosium Triangle: The Archetype of the Noncollinear Ising Model, *Physical Review Letters*, 2008, **100**, 247205.
15. F. S. Guo, B. M. Day, Y. C. Chen, M. L. Tong, A. Mansikkamaki and R. A. Layfield, Magnetic hysteresis up to 80 kelvin in a dysprosium metallocene single-molecule magnet, *Science*, 2018, **362**, 1400-1403.
16. K. S. Pedersen, A. M. Ariciu, S. McAdams, H. Weihe, J. Bendix, F. Tuna and S. Piligkos, Toward Molecular 4f Single-Ion Magnet Qubits, *J Am Chem Soc*, 2016, **138**, 5801-5804.
17. M. Shiddiq, D. Komijani, Y. Duan, A. Gaita-Ariño, E. Coronado and S. Hill, Enhancing coherence in molecular spin qubits via atomic clock transitions, *Nature*, 2016, **531**, 348-351.
18. M. Urdampilleta, S. Klyatskaya, J. P. Cleuziou, M. Ruben and W. Wernsdorfer, Supramolecular spin valves, *Nature Materials*, 2011, **10**, 502-506.
19. M. Shiddiq, D. Komijani, Y. Duan, A. Gaita-Arino, E. Coronado and S. Hill, Enhancing coherence in molecular spin qubits via atomic clock transitions, *Nature*, 2016, **531**, 348-351.
20. C. D. Buch, S. H. Hansen, D. Mitcov, C. M. Tram, G. S. Nichol, E. K. Brechin and S. Piligkos, Design of pure heterodinuclear lanthanoid cryptate complexes, *Chemical Science*, 2021, **12**, 6983-6991.
21. D. Aguilà, L. A. Barrios, V. Velasco, O. Roubeau, A. Repollés, P. J. Alonso, J. Sesé, S. J. Teat, F. Luis and G. Aromí, Heterodimetallic [LnLn'] Lanthanide Complexes: Toward a Chemical Design of Two-Qubit Molecular Spin Quantum Gates, *Journal of the American Chemical Society*, 2014, **136**, 14215-14222.
22. W. Wernsdorfer and M. Ruben, Synthetic Hilbert Space Engineering of Molecular Qudits: Isotopologue Chemistry, *Advanced Materials*, 2019, **31**, 1806687.
23. B. E. Bode, E. Fusco, R. Nixon, C. D. Buch, H. Weihe and S. Piligkos, Dipolar-Coupled Entangled Molecular 4f Qubits, *Journal of the American Chemical Society*, 2023, **145**, 2877-2883.
24. C. D. Buch, K. Kundu, J. J. Marbey, J. van Tol, H. Weihe, S. Hill and S. Piligkos, Spin-Lattice Relaxation Decoherence Suppression in Vanishing Orbital Angular Momentum Qubits, *J Am Chem Soc*, 2022, **144**, 17597-17603.
25. R. Hussain, G. Allodi, A. Chiesa, E. Garlatti, D. Mitcov, A. Konstantatos, K. S. Pedersen, R. De Renzi, S. Piligkos and S. Carretta, Coherent Manipulation of a Molecular Ln-Based Nuclear Qudit Coupled to an Electron Qubit, *J Am Chem Soc*, 2018, **140**, 9814-9818.
26. V. Rollano, M. C. de Ory, C. D. Buch, M. Rubín-Osanz, D. Zueco, C. Sánchez-Azqueta, A. Chiesa, D. Granados, S. Carretta, A. Gomez, S. Piligkos and F. Luis, High cooperativity coupling to nuclear spins on a circuit quantum electrodynamics architecture, *Communications Physics*, 2022, **5**.

27. R. Vincent, S. Klyatskaya, M. Ruben, W. Wernsdorfer and F. Balestro, Electronic read-out of a single nuclear spin using a molecular spin transistor, *Nature*, 2012, **488**, 357-360.
28. S. Thiele, F. Balestro, R. Ballou, S. Klyatskaya, M. Ruben and W. Wernsdorfer, Electrically driven nuclear spin resonance in single-molecule magnets, *Science*, 2014, **344**, 1135-1138.
29. A. Gaita-Ariño, F. Luis, S. Hill and E. Coronado, Molecular spins for quantum computation, *Nature Chemistry*, 2019, **11**, 301-309.
30. N. F. Chilton, Molecular Magnetism, *Annual Review of Materials Research*, 2022, **52**, 79-101.
31. J. G. C. Kragskow, J. Marbey, C. D. Buch, J. Nehrkorn, M. Ozerov, S. Piligkos, S. Hill and N. F. Chilton, Analysis of vibronic coupling in a 4f molecular magnet with FIRMS, *Nat Commun*, 2022, **13**, 825.
32. S. Takahashi, I. S. Tupitsyn, J. van Tol, C. C. Beedle, D. N. Hendrickson and P. C. E. Stamp, Decoherence in crystals of quantum molecular magnets, *Nature*, 2011, **476**, 76-79.
33. K. N. Shrivastava, Theory of Spin–Lattice Relaxation, *physica status solidi (b)*, 1983, **117**, 437-458.
34. M. J. Graham, C.-J. Yu, M. D. Krzyaniak, M. R. Wasielewski and D. E. Freedman, Synthetic Approach To Determine the Effect of Nuclear Spin Distance on Electronic Spin Decoherence, *Journal of the American Chemical Society*, 2017, **139**, 3196-3201.
35. L. J. Berliner, G. R. Eaton and S. S. Eaton, *Distance measurements in biological systems by EPR*, Kluwer Academic/Plenum Publishers, New York, 2000.
36. K. Bader, D. Dengler, S. Lenz, B. Endeward, S.-D. Jiang, P. Neugebauer and J. van Slageren, Room temperature quantum coherence in a potential molecular qubit, *Nature Communications*, 2014, **5**, 5304.
37. M. Atzori, E. Morra, L. Tesi, A. Albino, M. Chiesa, L. Sorace and R. Sessoli, Quantum Coherence Times Enhancement in Vanadium(IV)-based Potential Molecular Qubits: the Key Role of the Vanadyl Moiety, *Journal of the American Chemical Society*, 2016, **138**, 11234-11244.
38. C. E. Jackson, T. Ngendahimana, C.-Y. Lin, G. R. Eaton, S. S. Eaton and J. M. Zadrozny, Impact of Counter Ion Methyl Groups on Spin Relaxation in [V(C6H4O2)3]2–, *The Journal of Physical Chemistry C*, 2022, **126**, 7169-7176.
39. K. Bader, M. Winkler and J. van Slageren, Tuning of molecular qubits: very long coherence and spin–lattice relaxation times, *Chemical Communications*, 2016, **52**, 3623-3626.
40. J. D. Rinehart and J. R. Long, Exploiting single-ion anisotropy in the design of f-element single-molecule magnets, *Chemical Science*, 2011, **2**, 2078-2085.
41. J. J. Baldoví, S. Cardona-Serra, J. M. Clemente-Juan, E. Coronado, A. Gaita-Ariño and A. Palii, Rational Design of Single-Ion Magnets and Spin Qubits Based on Mononuclear Lanthanoid Complexes, *Inorganic Chemistry*, 2012, **51**, 12565-12574.
42. M. A. Sørensen, U. B. Hansen, M. Perfetti, K. S. Pedersen, E. Bartolomé, G. G. Simeoni, H. Mutka, S. Rols, M. Jeong, I. Zivkovic, M. Retuerto, A. Arauzo, J. Bartolomé, S. Piligkos, H. Weihe, L. H. Doerrer, J. van Slageren, H. M. Rønnow, K. Lefmann and J. Bendix, Chemical tunnel-splitting-engineering in a dysprosium-based molecular nanomagnet, *Nature Communications*, 2018, **9**, 1292.
43. E. Lucaccini, J. J. Baldovi, L. Chelazzi, A. L. Barra, F. Grepioni, J. P. Costes and L. Sorace, Electronic Structure and Magnetic Anisotropy in Lanthanoid Single-Ion Magnets with C(3) Symmetry: The Ln(trenovan) Series, *Inorg Chem*, 2017, **56**, 4729-4739.
44. A. Costache and A. M. Madalan, Mononuclear lanthanide(III) complexes with tripodal ligands as ammonium cation receptors, *Revue Roumaine de Chimie*, 2020, **65**, 761-765.
45. A. Falco, M. Neri, M. Melegari, L. Baraldi, G. Bonfant, M. Tegoni, A. Serpe and L. Marchiò, Semirigid Ligands Enhance Different Coordination Behavior of Nd and Dy Relevant to Their Separation and Recovery in a Non-aqueous Environment, *Inorganic Chemistry*, 2022, **61**, 16110-16121.
46. P. C. Vesborg, I. Chorkendorff, T. Brock-Nannestad, J. R. Dethlefsen and J. Bendix, Note: simple means for selective removal of the 365 nm line from the Hg spectrum using Dy, *Rev Sci Instrum*, 2011, **82**, 096102.
47. W. M. Haynes, *CRC Handbook of Chemistry and Physics*, 94th edn., 2014.
48. G. A. Bain and J. F. Berry, Diamagnetic Corrections and Pascal's Constants, *Journal of Chemical Education*, 2008, **85**, 532-536.
49. Bruker, *Bruker AXS, Inc. SAINT, Version 7.68A; Bruker AXS: Madison, WI, 2009*.
50. G. M. Sheldrick, *SADABS, Version 2008/2; University of Göttingen: Germany, 2003*.
51. G. M. Sheldrick, SHELXT - integrated space-group and crystal-structure determination, *Acta Crystallogr A Found Adv*, 2015, **71**, 3-8.
52. G. M. Sheldrick, Crystal structure refinement with SHELXL, *Acta Crystallogr C Struct Chem*, 2015, **71**, 3-8.
53. G. M. Sheldrick, A short history of SHELX, *Acta Crystallogr A*, 2008, **64**, 112-122.
54. O. V. Dolomanov, L. J. Bourhis, R. J. Gildea, J. A. K. Howard and H. Puschmann, OLEX2: a complete structure solution, refinement and analysis program, *Journal of Applied Crystallography*, 2009, **42**, 339-341.
55. L. J. Bourhis, O. V. Dolomanov, R. J. Gildea, J. A. Howard and H. Puschmann, The anatomy of a comprehensive constrained, restrained refinement program for the modern computing environment - Olex2 dissected, *Acta Crystallogr A Found Adv*, 2015, **71**, 59-75.
56. M. Kanesato, S. Mizukami, H. Houjou, H. Tokuhisa, E. Koyama and Y. Nagawa, Comparison of the bond lengths for the lanthanide complexes of tripodal heptadentate ligands, *Journal of Alloys and Compounds*, 2004, **374**, 307-310.
57. P. V. Bernhardt, B. M. Flanagan and M. J. Riley, Rapid Communication: Completion of the Isomorphous Ln(trensal) Series, *Australian Journal of Chemistry*, 2001, **54**.
58. K. S. Pedersen, J. Dreiser, H. Weihe, R. Sibille, H. V. Johannesen, M. A. Sørensen, B. E. Nielsen, M. Sigrist, H. Mutka, S. Rols, J. Bendix and S. Piligkos, Design of Single-Molecule Magnets: Insufficiency of the Anisotropy Barrier as the Sole Criterion, *Inorganic Chemistry*, 2015, **54**, 7600-7606.
59. C. D. Buch, S. H. Hansen, C. M. Tram, D. Mitcov and S. Piligkos, Functionalized Trigonal Lanthanide Complexes: A New Family of 4f Single-Ion Magnets, *Inorg Chem*, 2020, **59**, 16328-16340.

60. C. D. Buch, D. Mitcov and S. Piligkos, Lanthanide cryptate monometallic coordination complexes, *Dalton Trans*, 2020, **49**, 13557-13565.
61. K. S. Pedersen, J. Dreiser, H. Weihe, R. Sibille, H. V. Johannesen, M. A. Sorensen, B. E. Nielsen, M. Sigrist, H. Mutka, S. Rols, J. Bendix and S. Piligkos, Design of Single-Molecule Magnets: Insufficiency of the Anisotropy Barrier as the Sole Criterion, *Inorg Chem*, 2015, **54**, 7600-7606.
62. S. Stoll and A. Schweiger, EasySpin, a comprehensive software package for spectral simulation and analysis in EPR, *Journal of Magnetic Resonance*, 2005, **178**, 42-55.
63. D. Goldfarb and S. Stoll, *EPR Spectroscopy: Fundamentals and Methods*, Wiley, 2018.
64. D. Reta and N. F. Chilton, Uncertainty estimates for magnetic relaxation times and magnetic relaxation parameters, *Physical Chemistry Chemical Physics*, 2019, **21**, 23567-23575.
65. W. J. A. Blackmore, G. K. Gransbury, P. Evans, J. G. C. Kragskow, D. P. Mills and N. F. Chilton, Characterisation of magnetic relaxation on extremely long timescales, *Physical Chemistry Chemical Physics*, 2023, **25**, 16735-16744.
66. S. K. Hoffmann and S. Lijewski, Raman electron spin–lattice relaxation with the Debye-type and with real phonon spectra in crystals, *Journal of Magnetic Resonance*, 2013, **227**, 51-56.